Available online at www.sciencedirect.com
ScienceDirect
Polymer 47 (2006) 8604–8617
polymer
www.elsevier.com/locate/polymer

A new multiscale modeling approach for the prediction of mechanical properties of polymer-based nanomaterials

Stephan A. Baeurle [a,b,c,*], Takao Usami [d], Andrei A. Gusev [e]

[a] *Department of Chemistry and Pharmacy, Institute of Physical and Theoretical Chemistry, University of Regensburg, Universitaetstr. 31, D-93053 Regensburg, Bavaria, Germany*
[b] *Materials Research Laboratory, University of California, Santa Barbara, CA 93106, USA*
[c] *Department of Civil, Environmental and Geomatic Engineering, Institute for Building Materials, ETH, CH-8093 Zurich, Switzerland*
[d] *Polymer Design Laboratory, Mitsubishi Chemical Group Science and Technology Research Center, Yokkaichi, Mie 510-0885, Japan*
[e] *Department of Materials, Institute of Polymers, ETH, CH-8093 Zurich, Switzerland*

Received 5 September 2006; received in revised form 9 October 2006; accepted 16 October 2006
Available online 9 November 2006

Abstract

A detailed knowledge about the physics and chemistry of multiphase materials on different length and time scales is essential to tailor their macroscopic physical and mechanical properties. A better understanding of these issues is also highly relevant to optimize their processing and, thus, their elucidation can be decisive for their final industrial application. In this paper, we develop a new multiscale modeling method, which combines the self-consistent field theory approach with the kinetic Monte Carlo method, to simulate the structural–dynamical evolution taking place in thermoplastic elastomers, where hard glassy and soft rubbery phases alternate. Since the early seventies, it is well established that the properties of the core nanophases in these multiphase materials considerably affect their overall mechanical properties. However, recent experimental studies have clearly demonstrated that, besides the efficient handling of the core nanophases, the appropriate treatment of their interfacial region is another major challenge one has to face on the way of target-oriented development of these materials. In this work, we set a particular focus on the complex structural–dynamical processes occurring at the interphases, and study their influence on the local structural and mechanical properties. To reach our objectives, we apply the new methodology on a thermoplastic elastomer composed of ABA triblock copolymers, subjected to a sizeable external perturbation, and determine its time-averaged internal stress and composition profile. We deduce from this investigation that, to obtain the correct local mechanical properties of these multiphase materials, their structure and dynamics need to be taken into account on an equal footing. Finally, our investigation also provides an explanation and confirms the importance of the chain-pullout mechanism in the viscoelastic and stress relaxation behavior of these materials.

Keywords: Multiscale modeling of polymers; Mechanical properties; Interphases

1. Introduction

A long-standing challenge of physical, chemical and engineering sciences has been to develop theoretical tools for predicting structure and physical properties of polymer-based nanomaterials, like e.g. particulate filled polymer, polymer blends, nanostructured block copolymers, from the knowledge of a few input parameters. The need for such predictions has lately become increasingly important as new high-performance catalysts are now available that can produce many new exciting morphologies and macromolecular architectures [1–4]. It appears, however, that testing all possible material configurations for all their properties is often a very time- and cost-intensive task. To cope with the challenge,

* Corresponding author. Department of Chemistry and Pharmacy, Institute of Physical and Theoretical Chemistry, University of Regensburg, Universitaetstr. 31, D-93053 Regensburg, Bavaria, Germany. Tel.: +49 941 943 4470.
E-mail address: Stephan.Baeurle@chemie.uni-regensburg.de (S.A. Baeurle).

0032-3861/$ - see front matter © 2006 Elsevier Ltd. All rights reserved.
doi:10.1016/j.polymer.2006.10.017

several promising theoretical approaches have been devised recently that can open new perspectives for many new technological innovations [5–7]. However, despite these efforts, progress in the prediction of macroscopic physical properties from structure has only been slow in the past [8,9]. Major difficulties relate to the fact that (a) the microstructural elements in multiphase material are not shaped or oriented as in the idealizations of computer simulations, and more than one type can coexist [8]; (b) nonlinear properties damage the nanostructure, which leads to an uncharacterized new morphology that can change with time as further deformation and/or healing does occur [8]; (c) multiple length and time scales are generally involved and must be taken into account, when overall thermodynamic and mechanical properties wish to be determined [10]; and finally (d) the effect of the interphases and/or interfaces on the physical properties is often not well understood and characterized [11]. As a consequence, their role is often neglected in the development of new theoretical tools or they are treated in a very empirical way [12]. In this work, we focus on the understanding and efficient treatment of the latter two issues.

Some indications about the importance of interphases or interfaces in polymer-based nanomaterials have already been obtained through various experimental studies involving spectroscopic or mechanical measurements. From these investigations, it has been inferred that the impact of the interfacial regions on the overall mechanical properties becomes increasingly important with increasing mechanical perturbation imposed on the system. Such conclusions have, for example, been drawn by Diamant *et al.* [8] from tensile tests on thermoplastic elastomers (TPEs) composed of various phase-separated styrenic block copolymers. From the test results, these authors deduced that the linear or nonlinear mechanical perturbation leads to a stress concentration localized in the interfacial region between hard and soft nanophases. Moreover, they found that, if the interphase is diffuse with a small composition gradient, the domains are not in register and they fail individually, which explains that macroscopic yielding cannot be observed in this regime. In contrast, if the composition profile has a sharp gradient, high local stress concentrations are generated at the interphases, which causes that under a nonlinear strain all domains fail together in a cascade. In a later study, Henderson and Williams analyzed the issue of composition profiles at block copolymer interphases using experimental and theoretical approaches [13]. They showed that microphase-separated block copolymers generally possess asymmetric interphase regions, which are enriched by one of the components. Morèse-Séguéla *et al.* [14] deduced from their DSC- and ^{13}C NMR-line-width measurements on low molecular weight polystyrene–polyisoprene diblock copolymers that at the interphases there are indications for strong dynamical interactions between the chains in the soft and hard nanophases. They deduced that these interactions are responsible for the abnormal decrease of the glass-transition temperature, T_g, at the interphases, rather than a mixing of the two components assumed in previous works [15]. In a later work, Stöppelmann *et al.* [16] have shown evidences for an asymmetric density and motional profile of the chain segments at the interphases using ^{2}H-nuclear-magnetic-resonance spectroscopy. Very recently, Huy *et al.* [17] proposed that the interphases of tapered block copolymers can act as *stress absorbers*, which allow a more uniform stress distribution. All these experimental works indicate that the segmental structural dynamics, taking place at the interphases, is an important issue and its consequences on the macroscopic physical properties needs to be better understood.

In this work we investigate the complex structural–dynamical behavior of the chain segments involved in the interfacial region of TPE materials, composed of phase-separated styrenic triblock copolymers, and study its influence on the local mechanical properties. These multiphase materials are composed of triblock copolymer chains, where hard segments, made of polystyrene (PS), are chemically connected to soft segments, made of polyisoprene (PI) or polybutadiene (PB) [5,18]. For high molecular weights and below the order–disorder transition temperature, they phase-separate by forming a transient network of glass–rubber phases, where soft domains rich of either PB or PI and hard domains rich of PS alternate. Due to their exceptional strength and elasticity, these materials can be employed as high-performance elastomers and engineered to enhance the performance capabilities of a wide spectrum of end products and applications. To simulate their structural–dynamical evolution, we develop and apply a new multiscale modeling procedure based on the combination of the self-consistent-field theory (SCFT) approach and kinetic Monte Carlo (KMC) method, which is capable to treat the multiscale problem adequately and is able to reproduce the chain-dynamical processes occurring at the interphases.

Our paper is organized as follows. In Section 2.1 we introduce the model, describing the structural–dynamical process acting at the interphases of TPE materials, and discuss its relation to the glass model developed in one of our previous works [19]. Both pictures constitute the theoretical basis of our multiscale modeling approach. In Section 2.2 we describe how to modify the standard SCFT procedure, to mimic the characteristic glass phenomenon of dynamical arrest in the glassy phases on the chain level of description, while in Section 2.3 we introduce the KMC methodology and discuss how to compute the transition rates of the structural–dynamical process on the fly. In Section 2.4 we formulate our new multiscale modeling approach, which combines the previously introduced SCFT approach with the KMC algorithm. In Section 3 we demonstrate the suitability of our new algorithm for describing the structural–dynamical processes involved at the interphases of TPE materials. Finally, we end our paper with conclusions and a brief outlook.

2. Method

2.1. Structural–dynamical model

It is well established, since several decades, that a glassy polymer is the frozen state of an overcooled melt [20], in which the monomers are essentially trapped exhibiting a so-called

dynamical arrest [21]. In order to model a polymer in such a glassy state within the SCFT formalism, a simple solution is to freeze certain regions by keeping the monomers densities fixed in these regions and relax the chain configuration in the unconstrained rubbery phase by minimizing the overall free energy. Through the freezing procedure in the glassy phase, a new length and time scale is introduced into the system. For a more detailed discussion on the so-called ''frozen domains''-SCFT (FD-SCFT) method we refer to Section 2.2 and Appendix A. In a subsequent step, we calculate the internal elastic stress sustained by the polymer chains, using the Cauchy stress tensor formulation of Barrat *et al*. [22,23]. In polymeric liquids, the internal elastic stress is attributed to the intermolecular force between the polymer segments and is directly related to the orientation of the bond vectors [24]. To test the usefulness of this procedure, we apply our FD-SCFT method on a lamellar system of ABA triblock copolymers with alternating glass–rubber phases, subjected to an extensional strain of 8.3%. For the calculation, we use average volume fractions for the A and B monomers of $\bar{\phi}_{A|B} = 0.5$, a Flory–Huggins parameter of $\chi = 0.2$ and a polymerization index of $N = 100$, as well as a lattice spacing of $dx = 0.1$ in units of R_{g0}. In Fig. 1 we plot the internal stress of the glass–rubber system as a function of the grid number obtained from the calculation with our FD-SCFT method, in comparison to the internal stress and volume fractions of the A and B monomers obtained for the corresponding melt-like (rubber) system using the standard SCFT approach [25]. In our calculation, we have designated the areas on left- and right-hand side of the graph as pertaining to the melt-like phase, which is separated from the central glassy phase by broken lines. By considering the stress profile of the glass–rubber system, we observe that stress singularities appear at both sides of the glass–rubber interfaces and that they are in balance to each other. The singularities are due to the constrained alignment of the interfacial chain segments under the action of strain. Away from the interfaces, the stress decays rapidly, which relates to the fact that the chain segments are oriented at random in the bulk phases. In contrast, we observe that the curve obtained for the same copolymer system under melt conditions possesses a smooth behavior, as one should expect for a melt. Only a minor stress concentration appears in the interphase region, which is again due to the alignment of the interphase segments in the direction of strain. However, in contrast to the glass–rubber system, the interphase segments are now unconstrained. It is worth mentioning at this stage that the stress concentration at the static glass–rubber interfaces is a phenomenon one should expect from a physical point a few. Since the seminal work of Griffith in the early 1920s [26], it is well known that in materials with failures the stress is typically concentrated around the failure points. Griffith recognized that, when a nominal stress is applied to the external surface of a brittle material, the actual stress at the flaw can be many times the value of the externally applied stress and is typically amplified at the flaw's corner. Moreover, he found that the larger the flaw and the smaller its radius of curvature, the greater the enhancement of the stress at the flaw tip. In the same way, it has been inferred from fracture mechanics experiments with multiphase materials that the local stresses increase substantially near the interphase edges or corners [8]. In case of our glass–rubber system, treated with the FD-SCFT algorithm, the stress concentration takes place at the edges of *sharp* and *static* glass–rubber interfaces, as a consequence of the mechanical perturbation applied on the system. As a simple solution to cope with the stress concentration at these critical locations, one might first think about making use of a smoothing function. However, since the singularities are also critical in real systems, it is clear to us that with this procedure we would make our overall mechanical properties dependent on the choice of the smoothing function. A better solution to the problem is to take into account the fact that nature makes use of ingenious mechanisms, to reduce the sharpness of the interfaces and to avoid such high stresses. In general, on the molecular scale the structural properties are influenced by dynamical processes, which are the result of the correlated motion of the polymer chains. In case of our TPE system, this process might be a *glass–rubber interphase dynamics*, which causes that the system at the interfaces is in a transient state between melt and glass, leading to a softer interface profile. It appears to us reasonable to assume that this dynamical process can be described as a yielding process acting on the nanoscale, in which the material does undergo a transition from elastic to plastic deformation. The yielding deformation of glassy polymers is known to be driven by a thermally activated process and can conveniently be described by the theory of absolute reactions rates from chemical kinetics [20,27]. At the temperatures under consideration, this process can be viewed as a thermally activated slip-shear mechanism, considered to be the primary mechanism of plastic deformation in case of glassy polymers [20]. In the slip model of Zhu and Zhu [20], the slip-shear mechanism is described as the motion of relative sliding of neighboring monomers against the van-der-Waals (vdW) interactions. This

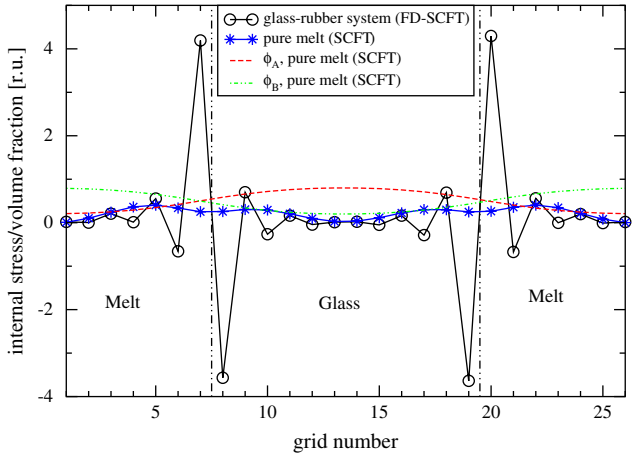

Fig. 1. Internal stress and volume fractions of the monomers as a function of the grid number for a lamellar system composed of phase-separated ABA triblock copolymers with alternating glassy and rubbery phases determined using the FD-SCFT algorithm, in comparison to the melt-like system determined with the standard SCFT algorithm.

picture has recently been confirmed experimentally by these authors on the example of glassy poly(methyl-methacrylate) (PMMA) [20] and by Swallowe and Lee for glassy PS [28]. Instead, at lower temperatures plastic deformation can also occur via alternative mechanisms, like e.g. thermally activated production of local molecular kinks [29] and/or the breaking of vdW bonds [30]. However, it is worth considering that these models are only phenomenological descriptions derived from experimental observations. To develop an adequate simulation procedure for the TPE materials under consideration, we need to formulate a consistent theoretical model of the glassy state within transition rates, which will provide us a theoretical basis for our KMC algorithm and give us an idea about the magnitude of the parameters, defining the thermally activated process.

In a recent work [19] we formulated and investigated a new glass theory, which could suitably reproduce the stress relaxation spectrum of TPEs, composed of phase-separated styrenic block copolymers. More specifically, we demonstrated that the crossover in the shift factors, observed experimentally to change from Williams–Landel–Ferry (WLF) to Arrhenius behavior crossing a characteristic temperature T^* and approaching the glass-transition temperature of the crosslinks from below, coincides with the crossover in behavior from power law to stretched exponential of the stress relaxation spectrum, found in recent tensile experiments [31]. We concluded from this work that a rate-determining thermally activated process determines the behavior of the glassy crosslinks in this temperature range, involving thermally activated breaking and re-forming of vdW bonds. We identified the characteristic temperature T^* to be identical with the second-order equilibrium transition temperature T_2 of the glassy PS phases. By combining a recently introduced theory for glasses of Di Marzio and Yang [32] with the significant-structure theory of Eyring and Ree [33], we developed a new glass theory, which is capable to describe the glassy state within transition rates and explain the characteristics of the mechanical behavior observed experimentally in these kind of materials. In this work, we also consider the thermally activated slip-shear motion via breaking and re-forming of vdW bonds to be the primary mechanism of deformation in the range of temperatures under investigation. This requires a more explicit consideration of the micromechanical process associated with slip-shear motion. In our view and in accordance with Zhu and Zhu [20], a glassy polymer is the frozen state of an overcooled melt, which can spatially be decomposed in elementary units containing polymer chains, held together by transient vdW bonds [19]. In the following, we will refer to these elementary units as activation units (AUs). In accordance with our recently proposed theory for glasses, we make use of a trapping description for elementary motion, in which escapes from deep energy wells provide the rate-determining steps. In Fig. 2 we show simplified sketches of the configuration space of our glass model in different temperature ranges, accessible within a typical experimental time frame. The points represent configurations of AUs and the connecting lines represent allowed transitions between the configurations. Configuration points belonging to

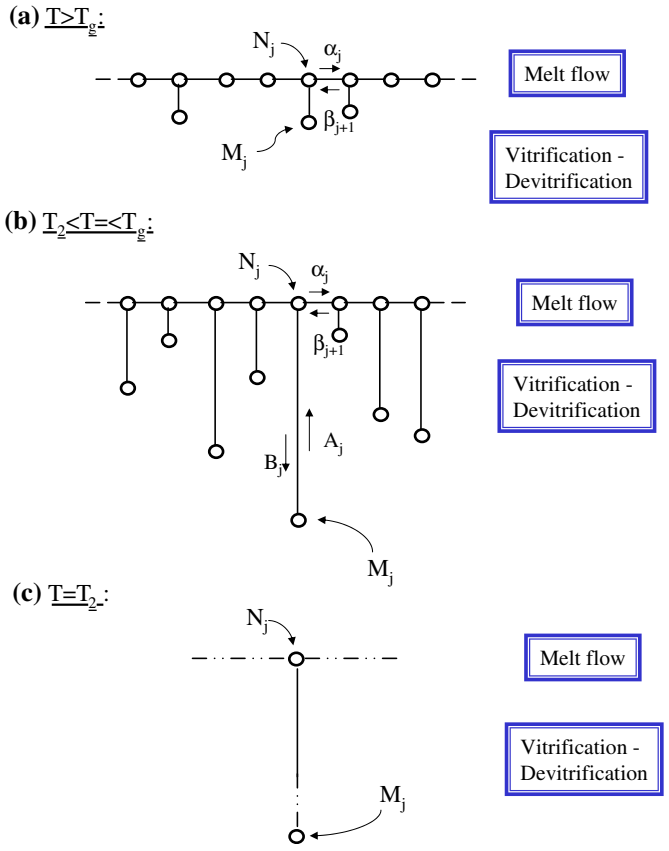

Fig. 2. Sketches of the underlying glass model at different temperature ranges.

the configurational sea of shallow energy wells are termed N_j and those belonging to the deep energy wells M_j. The horizontal lines with rates α_j for traveling to the right and β_{j+1} for traveling to the left designate motions of the configuration point among the configurational sea of shallow wells. The vertical lines connect the configurational sea to the deep wells, while the length of each vertical line is proportional to the potential energy depth of the well. The rate of escape from the deep wells is given by A_j and the rate of capture by B_j. When the configuration point is in a deep well, there is no motion. In Fig. 2(a) we show the configuration space of the glass-forming material at a temperature somewhat above T_g. In this regime, there are only a few deep wells relative to the number of shallow wells and the energy difference between them is rather small. As a consequence, the configuration point migrates rapidly from well to well within the configurational sea of shallow wells, and the system is able to flow or rearrange under the action of an external strain. In Fig. 2(b) the material is in the Arrhenius regime, characterized by the range of temperatures $T_2 < T \leq T_g$. In this situation, a configurational sea of shallow energy wells coexist with deep energy wells, and it is assumed that the jumps out of the deep wells are the rate-determining steps. Under these conditions, the material is solid like, but flows very slowly under the application of an external strain. If the configuration point is in one of the deep wells, it jumps out of it after a long period of time and wanders into the configurational sea of shallow wells,

until it falls into another low-lying well. It then stays in this well for another long period of time until it jumps out of it, repeating the process all over again. The rate-determining step in this picture is a simple vitrification/devitrification process without flow of matter, caused by the formation/breaking of transient bonds. Motion involving flow of matter occurs only when the configuration point has escaped and cruises around in the configurational sea of shallow wells and persists there until it falls into another low-lying well. In Fig. 2(c) we see the material's configuration space at T_2. At this temperature, there is only one configuration remaining, which is infinitely deep in energy, and, thus, the trajectory is trapped in the deep well. In this regime, the material has no freedom to rearrange and its viscosity diverges. Within this picture, the glass-transition phenomenon can now be explained by the appearance of *non-equilibrium spatio-temporal fluctuations* in vicinity to the glass transition, which lead to variations in the viscosity throughout the system and provoke the creation of *solid clusters* in the polymer melt. At T_g the system possesses the critical fraction of solid clusters with respect to the fraction of the melt-like regions, so that the solid clusters are able to connect to each other. This leads to the formation of a continuous rigid backbone, causing a sudden increase in the viscosity. In this situation, the system gets trapped in a *quasi-equilibrium state* by undergoing a *percolation transition*. Experimental evidences for the spatial–temporal heterogeneities in vicinity of T_g for glass-forming polymeric liquids have been accumulated over the past decade using experimental techniques, such as NMR, fluorescence recovery, dielectric hole burning or solvation dynamics [34].

Based on the glass model introduced previously, an algorithm can be proposed for the simulation of the slip-shear process, involved in the glassy crosslinks of styrenic TPE materials in the range of temperatures $T_2 < T \leq T_g(\mathrm{PS})$. It can be summarized with the following two-step procedure:

1. An AU is selected in space and the vdW bonds, acting between the styrenic monomers within an AU, are cooperatively formed or broken through thermal activation, depending on whether the AU is in a melt-like or solid state in its original configuration. The thermally activated process is efficiently mimicked via a KMC algorithm;
2. Under the action of strain on the AU, a subsequent step of flow motion of the chains is incorporated into the algorithm via minimization of the chain configuration within the molten (rubbery) phase.

To implement this algorithm, we treat the chains on the mesoscopic level of description using the FD-SCFT technique and combine it with a KMC algorithm, which allows to calculate the transition rates on the fly. Our procedure will be described in the subsequent sections.

2.2. SCFT with frozen domains

As we discussed in Section 2.1, we consider that the glassy state of an amorphous polymer can be described as the frozen state of an overcooled melt, in which the monomers are essentially trapped exhibiting a dynamical arrest. To mimic such a behavior within SCFT, let us consider in the following our TPE material, composed of phase-separated styrenic block copolymers. The partition function of this glass–rubber system can be expressed as [25]

$$\begin{aligned} Z = \int \mathrm{d}\vec{r}' \int \prod_{\alpha=1}^{n} \tilde{D}\vec{r}_\alpha \exp\left\{ -\rho_0^{-1} \int \mathrm{d}\vec{r}\, \chi \widehat{\rho}_\mathrm{A}(\vec{r}) \widehat{\rho}_\mathrm{B}(\vec{r}) \right\} \\ \times \delta\left[(1-\gamma(\vec{r}'))\left(\rho_\mathrm{rubb} - \widehat{\rho}_\mathrm{A} - \widehat{\rho}_\mathrm{B}\right)\right] \delta\left[\gamma(\vec{r}')\left(\rho_{\mathrm{A/glass}} - \widehat{\rho}_\mathrm{A}\right)\right] \\ \times \delta\left[\gamma(\vec{r}')\left(\rho_{\mathrm{B/glass}} - \widehat{\rho}_\mathrm{B}\right)\right], \end{aligned} \tag{1}$$

where $\widehat{\rho}_\mathrm{A}(\vec{r}) = N\sum_{\alpha=1}^{n}\int_0^f \mathrm{d}s\,\delta\left(\vec{r} - \vec{r}_\alpha(s)\right)$ and $\widehat{\rho}_\mathrm{B}(\vec{r}) = N\sum_{\alpha=1}^{n}\int_f^1 \mathrm{d}s\,\delta\left(\vec{r} - \vec{r}_\alpha(s)\right)$ are the monomer density operators for the A and B species, while f is the fraction of the polymer chain composed of A monomers. The total monomer density is $\rho_0 = nN/V$, where N is the polymerization index, n is the number of chains and V is the volume of the system. The integration measure $\tilde{D}\vec{r}_\alpha = D\vec{r}_\alpha \exp\left\{-1/4R_{\mathrm{g}0}^2 \int_0^1 \mathrm{d}s(\mathrm{d}\vec{r}_\alpha(s)/\mathrm{d}s)^2\right\}$, where $\int \tilde{D}\vec{r}_\alpha$ denotes a path integral over all possible conformations of the αth chain, represented by the space curve $\vec{r}_\alpha(s)$ and parameterized by the chain contour variable s. Moreover, the quantity R_{g0} designates the radius of gyration of the unperturbed chain. The step function $\gamma(\vec{r}')$ is 1 for $\vec{r}'$ in the glassy phase Ω_glass, while it is 0 otherwise. To mimic the dynamical arrest, we impose the following constraints $\widehat{\rho}_\mathrm{A}(\vec{r}) = \rho_{\mathrm{A/glass}}(\vec{r})$ and $\widehat{\rho}_\mathrm{B}(\vec{r}) = \rho_{\mathrm{B/glass}}(\vec{r})$ with $\rho_{\mathrm{A/glass}}(\vec{r}) + \rho_{\mathrm{B/glass}}(\vec{r}) = \rho_\mathrm{glass}$ on the monomer densities of the glassy phase, where $\rho_{\mathrm{A/glass}}(\vec{r})$ and $\rho_{\mathrm{B/glass}}(\vec{r})$ denote, respectively, the fixed values of the monomer densities of species A and B in this phase. In the rubbery phase Ω_rubb we impose the constrain $\rho_\mathrm{A}(\vec{r}) + \rho_\mathrm{B}(\vec{r}) = \rho_\mathrm{rubb}$, where ρ_rubb is the total density of monomers in the system, pertaining to the rubbery phase. Next, we convert the partition function into a field-theoretic formulation by making use of the functional integral identity $1 = \int D[\rho]\delta[\rho - \widehat{\rho}] = \int D[\rho]D[\nu] \exp\left\{\int \mathrm{d}\vec{r}\, \mathrm{i}\nu(\vec{r})\left[\rho(\vec{r}) - \widehat{\rho}(\vec{r})\right]\right\}$, where $\nu(\vec{r})$ is a field variable. The partition function, then, results in

$$Z = \int \mathrm{d}\vec{r}' \int D\rho_\mathrm{A} D\rho_\mathrm{B} Dw_\mathrm{A} Dw_\mathrm{B} Dp Du Dv \mathrm{e}^{-\beta F} \tag{2}$$

with the free energy

$$\begin{aligned} \beta F = \int \mathrm{d}\vec{r} \Big\{ \rho_0^{-1}\chi\rho_\mathrm{A}(\vec{r})\rho_\mathrm{B}(\vec{r}) - \mathrm{i}w_\mathrm{A}(\vec{r})\rho_\mathrm{A}(\vec{r}) \\ - \mathrm{i}w_\mathrm{B}(\vec{r})\rho_\mathrm{B}(\vec{r}) - \mathrm{i}p(\vec{r})[(1-\gamma(\vec{r}'))(\rho_\mathrm{rubb}(\vec{r}) \\ - \rho_\mathrm{A}(\vec{r}) - \rho_\mathrm{B}(\vec{r}))] - \mathrm{i}u(\vec{r})\left[\gamma(\vec{r}')\left(\rho_{\mathrm{A/glass}}(\vec{r}) \right.\right. \\ \left.\left. - \rho_\mathrm{A}(\vec{r})\right)\right] - \mathrm{i}v(\vec{r})\left[\gamma(\vec{r}')\left(\rho_{\mathrm{B/glass}}(\vec{r}) - \rho_\mathrm{B}(\vec{r})\right)\right] \Big\} \\ - n\ln Q\left[\mathrm{i}w_\mathrm{A}, \mathrm{i}w_\mathrm{B}; N\right], \end{aligned} \tag{3}$$

where

$$Q = \frac{\int \tilde{D}\vec{r}_\alpha \exp\left\{ -\int_0^f \mathrm{d}s\mathrm{i}Nw_\mathrm{A}(\vec{r}_\alpha(s)) - \int_f^1 \mathrm{d}s\mathrm{i}Nw_\mathrm{B}(\vec{r}_\alpha(s))\right\}}{\int \tilde{D}\vec{r}_\alpha} \tag{4}$$

denotes the single chain partition function and β the inverse temperature. The fields $p(\vec{r})$, $u(\vec{r})$ and $v(\vec{r})$ are responsible to enforce the density constraints discussed previously. Next, we perform the transformation $w \to \mathrm{i}Nw$, $p \to \mathrm{i}Np$, $u \to \mathrm{i}Nu$ and $v \to \mathrm{i}Nv$ and rewrite the modified free energy $\tilde{F} = \beta FN/(\rho_0 V)$ in terms of the volume fractions $\phi_i = \rho_i/\rho_0$. Moreover, we shift the free energy so that $F - F_0 = 0$ for $\omega_i = 0$, where F_0 is the free energy of the disordered phase. This provides the following expression for the free energy per chain:

$$\begin{aligned}\tilde{F} = V^{-1}\int \mathrm{d}\vec{r}\{&N\chi(\phi_\mathrm{A}(\vec{r}) - \bar{\phi}_\mathrm{A})(\phi_\mathrm{B}(\vec{r}) - \bar{\phi}_\mathrm{B}) \\ &- w_\mathrm{A}(\vec{r})\phi_\mathrm{A}(\vec{r}) - w_\mathrm{B}(\vec{r})\phi_\mathrm{B}(\vec{r}) - p(\vec{r})[(1-\gamma(\vec{r}'))\\ &\times(\rho_\mathrm{rubb}/\rho_0 - \phi_\mathrm{A}(\vec{r}) - \phi_\mathrm{B}(\vec{r}))] - u(\vec{r})[\gamma(\vec{r}')\\ &\times(\phi_{\mathrm{A/glass}}(\vec{r}) - \phi_\mathrm{A}(\vec{r}))] - v(\vec{r})[\gamma(\vec{r}')(\phi_{\mathrm{B/glass}}(\vec{r})\\ &- \phi_\mathrm{B}(\vec{r}))]\} - n\ln Q[\mathrm{i}w_\mathrm{A}, \mathrm{i}w_\mathrm{B}; N]\end{aligned} \tag{5}$$

with

$$Q = \frac{\int \tilde{D}\vec{r}_\alpha \exp\left\{ -\int_0^f \mathrm{d}sw_\mathrm{A}(\vec{r}_\alpha(s)) - \int_f^1 \mathrm{d}sw_\mathrm{B}(\vec{r}_\alpha(s))\right\}}{\int \tilde{D}\vec{r}_\alpha}, \tag{6}$$

where $\bar{\phi}_\mathrm{A}$ and $\bar{\phi}_\mathrm{B}$ are the average volume fractions of the A and B species, respectively. In the rubbery phase Ω_rubb we update the chemical potential fields from relaxation step n to $n+1$ in the following way:

$$\begin{aligned} w_\mathrm{A}^{n+1} - w_\mathrm{A}^n &= \lambda'\frac{\delta\tilde{F}}{\delta\phi_\mathrm{B}^n} + \lambda\frac{\delta\tilde{F}}{\delta\phi_\mathrm{A}^n} = \lambda'\left[\phi_\mathrm{A}^n - \bar{\phi}_\mathrm{A} - \frac{\omega_\mathrm{B}^n - p^n}{\chi N}\right] \\ &\quad + \lambda\left[\phi_\mathrm{B}^n - \bar{\phi}_\mathrm{B} - \frac{\omega_\mathrm{A}^n - p^n}{\chi N}\right], \\ w_\mathrm{B}^{n+1} - w_\mathrm{B}^n &= \lambda\frac{\delta\tilde{F}}{\delta\phi_\mathrm{B}^n} + \lambda'\frac{\delta\tilde{F}}{\delta\phi_\mathrm{A}^n} = \lambda\left[\phi_\mathrm{A}^n - \bar{\phi}_\mathrm{A} - \frac{\omega_\mathrm{B}^n - p^n}{\chi N}\right] \\ &\quad + \lambda'\left[\phi_\mathrm{B}^n - \bar{\phi}_\mathrm{B} - \frac{\omega_\mathrm{A}^n - p^n}{\chi N}\right], \end{aligned} \tag{7}$$

while in the glassy phase Ω_glass the fields are updated as follows:

$$\begin{aligned} w_\mathrm{A}^{n+1} - w_\mathrm{A}^n &= \lambda'\frac{\delta\tilde{F}}{\delta\phi_\mathrm{B}^n} + \lambda\frac{\delta\tilde{F}}{\delta\phi_\mathrm{A}^n} = \lambda'\left[\phi_\mathrm{A}^n - \bar{\phi}_\mathrm{A} - \frac{\omega_\mathrm{B}^n - v^n}{\chi N}\right] \\ &\quad + \lambda\left[\phi_\mathrm{B}^n - \bar{\phi}_\mathrm{B} - \frac{\omega_\mathrm{A}^n - u^n}{\chi N}\right], \\ w_\mathrm{B}^{n+1} - w_\mathrm{B}^n &= \lambda\frac{\delta\tilde{F}}{\delta\phi_\mathrm{B}^n} + \lambda'\frac{\delta\tilde{F}}{\delta\phi_\mathrm{A}^n} = \lambda\left[\phi_\mathrm{A}^n - \bar{\phi}_\mathrm{A} - \frac{\omega_\mathrm{B}^n - v^n}{\chi N}\right] \\ &\quad + \lambda'\left[\phi_\mathrm{B}^n - \bar{\phi}_\mathrm{B} - \frac{\omega_\mathrm{A}^n - u^n}{\chi N}\right], \end{aligned} \tag{8}$$

with the relaxation parameters chosen such that $\lambda' < \lambda$ and $\lambda > 0$. The volume fractions ϕ_A^n and ϕ_B^n are calculated via

$$\begin{aligned} \phi_\mathrm{A}^n(\vec{r}) &= \frac{1}{Q}\int_0^f \mathrm{d}sq(\vec{r},s)q^\dagger(\vec{r},s), \\ \phi_\mathrm{B}^n(\vec{r}) &= \frac{1}{Q}\int_f^1 \mathrm{d}sq(\vec{r},s)q^\dagger(\vec{r},s), \end{aligned} \tag{9}$$

where $q(\vec{r},s)$ is a restricted chain partition function that can be computed numerically as the solution to the modified diffusion equation

$$\frac{\partial q}{\partial s} = \begin{cases} R_{\mathrm{g}0}^2\nabla^2 q(\vec{r},s) - \mathrm{i}N\omega_\mathrm{A}q(\vec{r},s), & 0 < s < f, \\ R_{\mathrm{g}0}^2\nabla^2 q(\vec{r},s) - \mathrm{i}N\omega_\mathrm{B}q(\vec{r},s), & f < s < 1, \end{cases} \tag{10}$$

subjected to the initial condition $q(\vec{r},0) = 1$. The restricted partition function $q^\dagger(\vec{r},s)$ may be calculated as the solution to a modified diffusion equation similar to Eq. (10) with the right-hand side multiplied by -1, subjected to the initial condition $q^\dagger(\vec{r},1) = 1$ [35]. Having determined the restricted chain partition function, the single chain partition function can easily be obtained via

$$Q = V^{-1}\int \mathrm{d}\vec{r}q(\vec{r},1). \tag{11}$$

It can easily be demonstrated that in the rubbery phase Ω_rubb the value of the chemical potential fields at the saddle point satisfy the following set of equations:

$$\begin{aligned} w_\mathrm{A}(\vec{r}) &= \chi N(\phi_\mathrm{B}(\vec{r}) - \bar{\phi}_\mathrm{B}) + p(\vec{r}), \\ w_\mathrm{B}(\vec{r}) &= \chi N(\phi_\mathrm{A}(\vec{r}) - \bar{\phi}_\mathrm{A}) + p(\vec{r}), \end{aligned} \tag{12}$$

whereas the pressure field obeys

$$p(\vec{r}) = (w_\mathrm{A}(\vec{r}) + w_\mathrm{B}(\vec{r}))/2 - \chi N\bar{\phi}_\mathrm{rubb}/2. \tag{13}$$

In contrast, in the glassy phase Ω_glass at the saddle point the chemical potential fields satisfy equations

$$\begin{aligned} w_\mathrm{A}(\vec{r}) &= \chi N(\phi_\mathrm{B}(\vec{r}) - \bar{\phi}_\mathrm{B}) + u(\vec{r}), \\ w_\mathrm{B}(\vec{r}) &= \chi N(\phi_\mathrm{A}(\vec{r}) - \bar{\phi}_\mathrm{A}) + v(\vec{r}), \end{aligned} \tag{14}$$

whereas the fields of the density constraints obey

$$\begin{aligned} u(\vec{r}) &= w_\mathrm{A}(\vec{r}) - \chi N\phi_{\mathrm{B/glass}}(\vec{r}), \\ v(\vec{r}) &= w_\mathrm{B}(\vec{r}) - \chi N\phi_{\mathrm{A/glass}}(\vec{r}). \end{aligned} \tag{15}$$

The relaxation scheme for calculating the saddle point values for the fields is given by the following steps:

1. Set the random initial values for w_A, w_B and p;
2. Solve the modified diffusion equations numerically to calculate $q(\vec{r},s)$ and $q^\dagger(\vec{r},s)$;
3. Substitute these functions into Eq. (9) to obtain ϕ_A^n, ϕ_B^n;
4. Use the chemical potential field expressions in Eqs. (7) and (8), to update the chemical potential fields at the nth iteration, w^n, to their values at the $(n+1)$ iteration, w^{n+1};
5. Update the pressure field in the rubbery phase Ω_rubb via Eq. (13) and the fields of the density constraints of the glassy phase Ω_glass via Eq. (15).

In order to determine the total density of rubbery monomers in the system $\bar{\phi}_{\mathrm{rubb}}$ required in Eq. (13), we consider that the overall system is incompressible. This means that an increase of the total monomer density in the glassy phase is compensated by a decrease of the total monomer density in the rubbery phase upon deformation, without formation of microvoids. Such a mechanism has been established experimentally by Michler *et al.* using nanoanalytical techniques based on electron and atomic force microscopy [36]. To demonstrate the procedure, let us consider the average volume fractions of the A and B monomers contained in the overall system of volume V

$$\begin{aligned}\bar{\phi}_{\mathrm{A}} &= \frac{1}{V}\Big[\int_{\Omega_{\mathrm{glass}}} \phi_{\mathrm{A}}(\vec{r})\mathrm{d}\vec{r} + \int_{\Omega_{\mathrm{rubb}}} \phi_{\mathrm{A}}(\vec{r})\mathrm{d}\vec{r}\Big],\\ \bar{\phi}_{\mathrm{B}} &= \frac{1}{V}\Big[\int_{\Omega_{\mathrm{glass}}} \phi_{\mathrm{B}}(\vec{r})\mathrm{d}\vec{r} + \int_{\Omega_{\mathrm{rubb}}} \phi_{\mathrm{B}}(\vec{r})\mathrm{d}\vec{r}\Big],\end{aligned} \tag{16}$$

where $\bar{\phi}_{\mathrm{A/B}} = \bar{\rho}_{\mathrm{A/B}}/\rho_0$. Summing both expressions, we get

$$\bar{\phi}_{\mathrm{A}} + \bar{\phi}_{\mathrm{B}} = \frac{1}{V}\Bigg[\int_{\Omega_{\mathrm{glass}}} \big[\phi_{\mathrm{A}}(\vec{r}) + \phi_{\mathrm{B}}(\vec{r})\big]\mathrm{d}\vec{r} + \int_{\Omega_{\mathrm{rubb}}} \big[\phi_{\mathrm{A}}(\vec{r}) + \phi_{\mathrm{B}}(\vec{r})\big]\mathrm{d}\vec{r}\Bigg] = 1. \tag{17}$$

To introduce the hard-core repulsion between the monomers in the rubbery phase, we assume that the total density of monomers in the rubbery phase is locally constant, i.e. $\phi_{\mathrm{A}}(\vec{r}) + \phi_{\mathrm{B}}(\vec{r}) = \bar{\phi}_{\mathrm{rubb}}$ in Ω_{rubb}. This implies

$$\int_{\Omega_{\mathrm{rubb}}} \big[\phi_{\mathrm{A}}(\vec{r}) + \phi_{\mathrm{B}}(\vec{r})\big]\mathrm{d}\vec{r} = V_{\mathrm{rubb}}\bar{\phi}_{\mathrm{rubb}}, \tag{18}$$

where $\bar{\phi}_{\mathrm{rubb}} = \bar{\rho}_{\mathrm{rubb}}/\rho_0$ and V_{rubb} is the volume of the rubbery phase. Inserting Eq. (18) into Eq. (17), we obtain the average volume fraction of the rubbery monomers in the system as

$$\bar{\phi}_{\mathrm{rubb}} = \frac{1}{V_{\mathrm{rubb}}}\Bigg[V - \int_{\Omega_{\mathrm{glass}}} \big[\phi_{\mathrm{A}}(\vec{r}) + \phi_{\mathrm{B}}(\vec{r})\big]\mathrm{d}\vec{r}\Bigg]. \tag{19}$$

The local volume fractions of the glassy monomers $\phi_{\mathrm{A/glass}}(\vec{r})$ and $\phi_{\mathrm{B/glass}}(\vec{r})$, needed in Eq. (15), are obtained preliminary to the simulation by using the values of the corresponding melt-like system, calculated with the standard SCFT approach [25].

2.3. Kinetic Monte Carlo algorithm

In a large class of systems the dynamic evolution is inherently stochastic, and changes in the local configuration occur concertedly in space and time. The kinetic Monte Carlo KMC method is an extremely efficient method to carry out dynamical simulations of such stochastic and/or thermally activated processes, when the relevant micromechanical mechanisms determining the dynamical evolution are known. KMC simulations have successfully been used to model a variety of dynamical processes, ranging from catalysis to thin film growth [37–39]. The approach has also widely been employed to simulate the deformation behavior of polymer systems [40].

To outline the basic principle of the KMC method, let us consider a system containing N possible transition events, among which each event i is associated with a rate r_i [39], determining the dynamics of barrier crossing on the potential energy surface. For this system a list of rates $\mathbf{R} = \{r_1, r_2, \ldots, r_N\}$ can be constituted and a particular configuration of the system at a particular time can be characterized by the distribution of the N events over the rates $\mathbf{R}$. This distribution is constructed by a MC algorithm, which selects randomly among various possible events available at each time and effects the events with appropriate transition probabilities $\mathbf{W} = \{w_1, w_2, \ldots, w_N\}$. To ensure that a direct and unambiguous relationship between Monte Carlo time and real time is established [39], the transition probabilities must be constructed in such a way that a *dynamical hierarchy* of transition rates is preserved away from equilibrium. Generally stated, a dynamical hierarchy of transition probabilities is created when a probability for a transition i is defined as

$$w_i = \frac{r_i}{\xi_{\max}}, \tag{20}$$

where r_i is the rate at which event i occurs and $\xi_{\max}$ is a number obeying the condition $\xi_{\max} \geq \sup\{r_i\}$. The creation of a dynamical hierarchy of transition rates ensures that transition probabilities are uniquely defined. For example, a dynamical hierarchy is not achieved in case of the standard Metropolis algorithm useful for systems near equilibrium, because all transitions of the system to lower or equivalent energy states are considered to have a probability of unity [41]. Another important requirement is that time increments upon successful events should be calculated appropriately, i.e. time at each trial i, at which an event is realized, should be updated with an increment τ_i selected from an exponential distribution,

$$\tau_i = -\frac{1}{\sum_{i=1}^{N} r_i}\ln(\xi), \tag{21}$$

where ξ is a uniform random number between 0 and 1. Finally, if in addition the various events can be supposed to be independent, then the MC algorithm simulates a Poisson process [39], and the MC trajectory mimics real time dynamics. A simple implementation, obeying the previous requirements, is known as the Bortz–Kalos–Lebowitz (BKL) algorithm [37] and can be summarized by the following steps:

1. Set the time $t = 0$;
2. Form a list of all the rates r_j of all N possible transitions in the system. Any transition j can only occur one time and is carried out with a rate r_j;
3. Calculate the cumulative functions $R_i = \sum_{j=1}^{i} r_j$ for $i = 1, \ldots, N$;
4. Get a uniform random number $\xi \in [0, 1]$;
5. Pick an event i randomly and, then, let it occur with a probability

$$w_i = \frac{r_i}{R_N} \tag{22}$$

by finding the i for which

$$R_{i-1}/R_N < \xi \leq R_i/R_N; \tag{23}$$

6. Carry out event i;
7. Recalculate all transition rates r_i, which may have changed due to the transition;
8. Get a new uniform random number $\xi \in [0, 1]$;
9. Update the time via

$$t = t + \tau_i, \tag{24}$$

where

$$\tau_i = -\frac{\ln \xi}{R_N}; \tag{25}$$

10. Return to step (1).

We point out that by defining the transition probabilities w_i according to Eq. (22) the dynamical hierarchy criterion is automatically satisfied [39]. Moreover, it is worth considering from a mathematical point of view that the BKL algorithm can be regarded as an algorithm that numerically solve the Master equation

$$\frac{\partial p(\lambda,t)}{\partial t} = \sum_{\lambda'} w(\lambda' \to \lambda) p(\lambda',t) - \sum_{\lambda} w(\lambda \to \lambda') p(\lambda,t), \tag{26}$$

where λ and λ' are successive states of the system, $p(\lambda, t)$ is the probability that the system is in state λ at time t and $w(\lambda' \to \lambda)$ is the probability per unit time that the system will undergo a transition from state λ' to state λ. At a steady state (not necessarily at equilibrium), the time derivative on the left-hand side of Eq. (26) is zero and, consequently, the sum of all transitions into a particular state λ become equal to the sum of all transitions out of that state. To fulfill this condition, one must require that the phenomenological model obeys the detailed balance criterion

$$w(\lambda' \to \lambda) p(\lambda', t = \infty) = w(\lambda \to \lambda') p(\lambda, t = \infty), \tag{27}$$

in which

$$p(\lambda, t = \infty) = Z^{-1} \mathrm{e}^{-\beta H(\lambda)}. \tag{28}$$

It is imposed to ensure that the MC transition probabilities are chosen in such way that the system converges to the limiting distribution $p(\lambda, t = \infty)$, consistent with the model Hamiltonian $H(\lambda)$ and the partition function Z of the system. Summing over all states λ' in Eq. (27) and considering that the total probability

$$\sum_{\lambda'} w(\lambda' \to \lambda) = 1, \tag{29}$$

we get [41]

$$\sum_{\lambda'} w(\lambda' \to \lambda) p(\lambda', t = \infty) = p(\lambda, t = \infty). \tag{30}$$

We see that, by imposing the conditions (27) and (29), we achieve that the transition probabilities satisfy the eigenvalue equation given in Eq. (30), characterizing a Markov chain with a limiting distribution $p(\lambda, t = \infty)$. Now, in order to realize detailed balance in a KMC algorithm, the transition probabilities of the forward and backward thermally activated process can be defined as follows:

$$\begin{aligned} w(\lambda \to \lambda') &\propto \mathrm{e}^{-\beta\epsilon}, \\ w(\lambda' \to \lambda) &\propto \mathrm{e}^{-\beta(\Delta E + \epsilon)}, \end{aligned} \tag{31}$$

where $\Delta E = H(\lambda) - H(\lambda')$ is the energy difference between the initial and final state λ' and λ, while ϵ and $\Delta E + \epsilon$ are the activation barriers of the forward and backward process, respectively. Finally, by inserting Eqs. (31) and (28) into Eq. (27), we can easily convince ourselves that the detailed balance criterion is satisfied. Further, normalizing the transition probabilities according to Eq. (29) guarantees that the Markov chain converges to the limiting distribution $p(\lambda, t = \infty)$. To conclude, it is worth mentioning that the BKL algorithm can be used to simulate a system in equilibrium as well as out of equilibrium, as long as it fulfills the basic criteria given previously. Moreover, because in the BKL algorithm the list of transition probabilities are recalculated within every iteration step, the simulation process can be modified at every iteration.

2.4. Combined KMC–SCFT algorithm

In the following we describe how to combine the SCFT and KMC algorithm introduced previously, which will permit to simulate the structural–dynamical model described in Section 2.1 on the chain level of description. Its basic steps are visualized in Fig. 3. In the preliminary step we discretize the simulation cell in AUs and determine the initial configuration of frozen AUs in the system. This is achieved by minimizing the free energy $\tilde{F}$ of the copolymer melt and calculating its initial phase-separated morphology using the standard SCFT approach [25], providing initial fields and volume fractions of the A and B monomers. The procedure delivers a fully relaxed and unstrained morphology, and the phases designated as the glassy phases can now be frozen by fixing their respective volume fractions locally. In a subsequent step an external strain may be imposed and the partially frozen system is allowed to relax to mechanical equilibrium by minimizing its free energy $\tilde{F}$, given by Eq. (5). From this new configuration, the local stresses, fields and volume fractions on the grid are determined. Next, the KMC procedure is started by generating the list of possible transition events, $n = 1, \ldots, N$, for the given configuration of AUs $\{\lambda\}$ with stress distribution $\{\sigma\}$ and by calculating the transition rate, r_n, of each event n. This list of events is constituted by the AUs that can either be in a vitrified or devitrified state. In our approach we allow only the boundary AUs at the glass–rubber interfaces to contribute to the configuration space. AUs of the melt phase are allowed to undergo with a certain transition probability the vitrification process, to become frozen AUs, while boundary AUs of the glassy phase are allowed to melt with a certain probability.

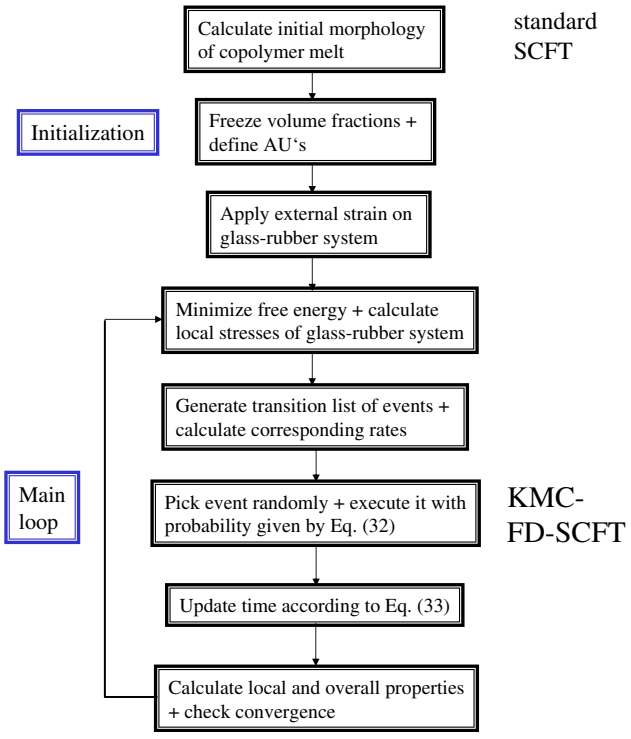

Fig. 3. Sketch showing the basic steps of the KMC–SCFT algorithm.

Having generated the transition list of possible events, an event n is picked with probability

$$p_n = \frac{r_n}{\sum_{i=1}^{N} r_i}. \tag{32}$$

The selected event is executed and time is advanced by

$$\tau = \frac{\ln(\xi)}{\sum_{i=1}^{N} r_i}. \tag{33}$$

Flow in the rubbery phase is allowed in a subsequent step through minimization of the free energy, which permits the rearrangement of the polymer chains. From this new configuration, the local and overall properties are determined. It is worth mentioning that equilibration through minimization is performed after each KMC step, since molecular rearrangements of the chains in the rubbery phase are much faster than the yielding process occurring in the glassy phase. Finally, the convergence with respect to the local and overall properties is checked.

In the following we define the basic properties of an AU and derive an expression for the associated thermally activated rate process. To define an AU, let us consider our TPE material composed of phase-separated ABA triblock copolymers. First of all, we determine the internal stresses with a standard SCFT calculation and discretize the system, characterized by a heterogeneous stress distribution, in elementary units, in which the stress is homogeneously distributed. By using the absolute theory of reaction rates [27] and taking into account the transition probabilities in Eq. (31), we can express the forward and backward transition rates of the thermally activated process associated with an AU as

$$\begin{aligned} r_{\rightarrow}^{\mathrm{AU}}(\vec{r}) &= r_0^{\mathrm{AU}} \exp\left[-\frac{\left(\Delta E^{\mathrm{AU}}(\vec{r}) - v^{\mathrm{AU}}(\vec{r})\sigma^{\mathrm{AU}}(\vec{r})\right)}{k_{\mathrm{B}}T}\right], \\ r_{\leftarrow}^{\mathrm{AU}}(\vec{r}) &= r_0^{\mathrm{AU}} \exp\left[-\frac{\left(\Delta E^{\mathrm{AU}}(\vec{r}) + v^{\mathrm{AU}}(\vec{r})\sigma^{\mathrm{AU}}(\vec{r})\right)}{k_{\mathrm{B}}T}\right], \end{aligned} \tag{34}$$

where r_0^{AU} is the thermal vibration frequency of the AU and k_{B} the Boltzmann constant, while $\Delta E^{\mathrm{AU}}(\vec{r})$ and $v^{\mathrm{AU}}(\vec{r})$ are the activation internal energy and activation volume of the AU, respectively. Let us consider in the following that the relaxation of the glassy phase of the TPE material is so slow, while cooling down from the melt during processing, that it is trapped in a quasi-equilibrium state and it adopts a constant *average temperature* $\bar{T}(t)$, which depends on time t. For further details we refer to Section 2.1 of our manuscript and Section 2.2 of Ref. [19]. Moreover, we assume that the system is thermalized by a heat bath of temperature T and that $\bar{T}(t) \approx T$, where we take into account that the time scale of the relaxation of the glassy phase is much larger than the time scale of the structural–dynamical process occurring at the interphases. The activation energy associated with a thermally activated process of an AU is, then, given by

$$\Delta E^{\mathrm{AU}}(\vec{r}) = U\rho_{\mathrm{KE}}(T)\phi_{\mathrm{A}}(\vec{r}), \tag{35}$$

where U is the height of the potential barrier for an individual vdW bond, which needs to be broken in the cooperative process in order to allow melting of the AU, and ϕ_{A} is the volume fraction of A monomers in our TPE material, responsible for glass-formation. The density of kinetic entities $\rho_{\mathrm{KE}}(\bar{T}(t))$, i.e. vdW bonds, in a hypothetical glass, only composed of A monomers, is given by our glass model as

$$\rho_{\mathrm{KE}}(T) = \frac{\bar{T}(t)}{N_{\mathrm{AU}}(\bar{T}(t) - T_2)} \approx \frac{T}{N_{\mathrm{AU}}(T - T_2)}, \tag{36}$$

where N_{AU} is the number of activation units and T_2 is the temperature, at which the viscosity diverges and the material becomes fully rigid. Moreover, on the basis of transition state theory [42], we interpret the activation volume of an AU, $v^{\mathrm{AU}}(\vec{r})$, as the difference in volumes of the activated and inactivated state. Since an AU can only adopt solid- or melt-like properties, we assume that the temperature dependence of the activation volume of an AU can be neglected. In this context, it is also worth considering that, to introduce temperature dependence into the algorithm in a consistent way, we also need to take into account the temperature dependence of the Flory–Huggins χ-parameter. This parameter is assumed to obey the following functional form [43]:

$$\chi\rho_0 = \frac{\gamma}{T} + \epsilon, \tag{37}$$

where γ and ϵ are constants. For the PS–PI interactions in our block copolymer system, we choose the coefficients in Eq. (37) to be $\gamma = 496\ \mathrm{Knm}^{-3}$ and $\epsilon = -0.595\ \mathrm{nm}^{-3}$ [43]. It is

worth emphasizing that the temperature dependence of the χ-parameter does not depend significantly on the method of determination, but its absolute value via the coefficients does [44]. In conclusion, we see that Eqs. (35), (36) and (37) in conjunction with Eq. (34) fully determine the time-dependent evolution of the system as a function of temperature.

Other possible micromechanisms of deformation are related to translation of entanglements and end points in space, like e.g. chain slippage across an entanglement, chain disentanglement, chain re-entanglement and chain scission. In our KMC–SCFT approach we consider that the yielding deformation is unaffected by the entanglement structure and, as a consequence, in our algorithm we neglect related micromechanical processes. This assumption is supported by the experimental work of Miller [45], who found in his investigation of low-molecular weight PS that the viscosity at the glass transition for samples with a molecular weight $M < 19\,300 = M_c$ is independent of the molecular weight and adopts a characteristic value of $\log\ \eta_g = 13 \pm 1$. This clearly shows that entanglements play no role in the viscosity of PS below M_c and that in this regime the viscosity is entirely determined by the vdW interactions between the monomers. However, when loading is carried beyond the yielding region, the load generally needs to increase for additional strain to occur. This effect is called strain hardening and is associated with an increased resistance to slip deformation of the entanglement structure of the polymer network [46]. In this regime thermally activated chain slippage and disentanglement processes need to be taken into account [12]. Another process, which can occur under heavy load conditions, is thermally activated chain scission of C–C bonds in the polymers [47]. Since this process occurs only under heavy load conditions, this effect is also neglected in our algorithm.

3. Results and discussion

We start our investigations by performing calculations with our combined KMC–SCFT approach for the TPE material considered in Section 2.1, where the FD-SCFT algorithm failed to provide useful results. In the calculations we considered a lamellar system composed of ABA triblock copolymers with alternating glass–rubber phases, subjected to an extensional strain of 8.3%. We used average volume fractions for the A and B monomers of $\bar{\phi}_{A|B} = 0.5$, a Flory–Huggins parameter of $\chi = 0.2$ and a polymerization index of $N = 100$, as well as a lattice spacing of $\mathrm{d}x = 0.1\ R_g$. In Fig. 4 we have visualized the fluctuations of both glass–rubber interfaces as a function of real time at four different temperatures below T_g(PS), i.e. $T = 305$ K, 320 K, 350 K and 380 K. From the graphs, we deduce that the interfaces fluctuate about some equilibrium average values at all temperatures and that the magnitude of the fluctuations as well as the frequency of events within a time interval grow with increasing temperature. The latter behavior can easily be explained physically by the increase of the transition rates for the processes of breaking and forming of the vdW bonds in the glassy phase as the kinetic energy in the system becomes larger. Next, in Fig. 5 we show the 1000-point

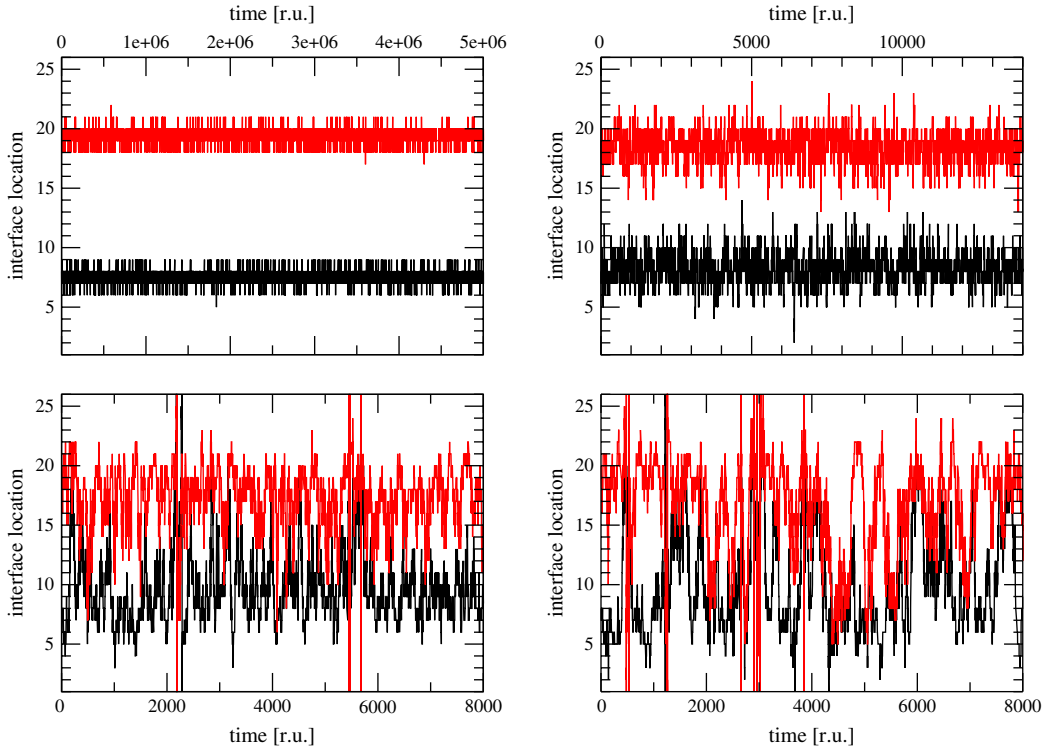

Fig. 4. Glass–rubber interface locations versus real time at various temperatures for the TPE material composed of ABA triblock copolymers, determined with the combined KMC–SCFT algorithm. In the calculations the following temperatures have been considered: $T = 305$ K (upper left), $T = 320$ K (upper right), $T = 350$ K (lower left) and $T = 380$ K (lower right).

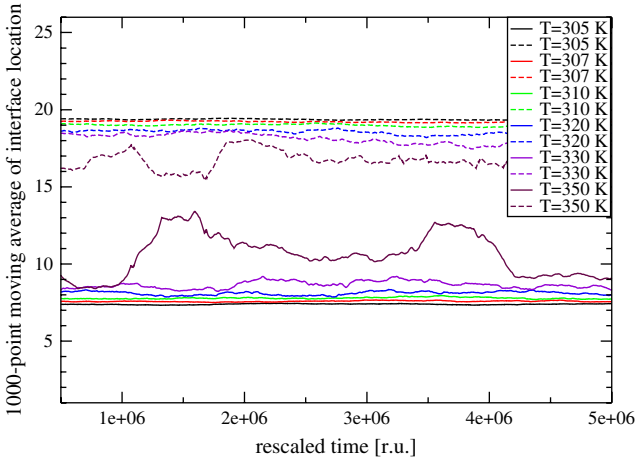

Fig. 5. 1000-Point moving average of the interface locations versus rescaled real time at various temperatures for the TPE material composed of ABA triblock copolymers, determined with the combined KMC–SCFT algorithm.

moving average of the interface location versus the rescaled real time at various temperatures. For a better visualization, we rescaled the time of the curves according to the following equation $t' = A_t(T)t$, where t' represents the rescaled time and $A_t(T)$ the scaling factor. The scaling factors are $A_t(T = 307\ \mathrm{K}) = 32$, $A_t(T = 310\ \mathrm{K}) = 135$, $A_t(T = 320\ \mathrm{K}) = 375$, $A_t(T = 330\ \mathrm{K}) = 480$, $A_t(T = 350\ \mathrm{K}) = 665$. We recognize that with increasing temperature the fluctuations become stronger and the glassy phase between both interfaces becomes narrower. This is due to the fact that the glassy phase melts successively due to the gradual change of the composition profile, which is associated with the gradual change of the glass-transition temperature. These results are in consistency with a series of experimental investigations from the late 1960s and early 1970s [48], from which it has been inferred that with increasing temperature the PS crosslinks in styrenic TPEs become softer. In these works a higher ductility of the PS glassy phase was reported at lower temperatures, than predictable from the values of the bulk material. In a subsequent study Morèse-Séguéla *et al.* [14] demonstrated, using DSC and ^{13}C NMR-line-width spectroscopy, that at the interphases of nanophase-separated low-molecular weight PS–PI diblock copolymers the glass-transition temperature changes gradually with the composition gradient. They assumed this behavior to be the result of strong dynamical interactions, taking place between the polymer chains in the soft and hard nanophases [15]. Their experimental findings have recently been confirmed by experimental investigations of Park *et al.* [49] on thin random copolymer films, who provided further evidences for the thickness and composition dependence of the glass-transition temperature of the hard nanophases. Note that, for demonstration purposes, we chose in our calculations, analogously as Morèse-Séguéla *et al.* in their experimental work, a low-molecular weight block copolymer with a large interphase region. Commercially used block copolymer materials, however, generally have a higher molecular weight and, thus, possess a very small interphase region, which is often hard to be detected. Next, we deduce from the figure that, approaching the glass-transition temperature of the crosslinks from below, there is an increased probability that the crosslinks melt for a short period of time, as a result of fluctuations. We can particularly well infer this from the curves, representing both interfaces, at a temperature of $T = 350$ K. In the time interval between $t' = 1 \times 10^6$ and 2×10^6, we see that the curves do almost touch each other, and we can safely predict that, if we would run the simulation for a longer time, instantaneous melting due to fluctuations would be very likely to occur. In the following we will call such a phenomenon *fluctuational melting* and emphasize that it has important consequences for the mechanical properties of these materials. This is due to the fact that, during the small time frame the crosslinks are in the molten state, the chains can partially or fully pull out of the crosslinks under the action of strain and in this way relax their stress. In contrast, at a temperature of $T = 305$ K, we see that the interface curves are far apart and fluctuate only slightly. In this situation it is very improbable that they will coincide over some time interval and that fluctuational melting can take place, even in a simulation run of infinite time. As a consequence, at this temperature the glassy crosslinks remain rigid, and the material does not flow under the action of strain on an accessible time scale. It is also worth noting in this context that the process of chain pullout has been suggested by Hotta *et al.* [31], to explain the viscoelastic and stress relaxation behavior of these materials, observed in their mechanical experiments in the range of temperatures $T_2 < T \leq T_g(\mathrm{PS})$. Its crucial role has recently been confirmed in a theoretical work of Baeurle *et al.* [10], who provided a theoretical foundation to their experimental results. Note that due to the restriction in computational time, we could not explicitly show such an instantaneous melting event here, but we plan to do extensive investigations on this phenomenon in a subsequent work. In the Figs. 6–8 we show the resulting time-averaged internal stress and volume fractions of the A and B monomers as a function of the grid number at three different temperatures, i.e. $T = 305$ K, 320 K and 350 K. We compare the curves obtained with increasing time to the static internal stress configuration obtained at $t = 0$. For a better visualization, we rescaled the static stress curve using $\sigma' = \sigma/2$. We recognize that the stress profile at $T = 305$ K still possesses a strong stress concentration at the interphases, even if the stress peaks are already significantly reduced compared to the static internal stress profile at $t = 0$, where no interphase dynamics is taken into account. By comparing the time-averaged stress profile at this temperature with the corresponding curves at higher temperatures in the subsequent graphs, we see that the stress peaks significantly decrease in magnitude with increasing temperature and that the double peaks at each interphase are replaced by single peaks. We also notice by considering the stress profiles at different times and temperatures that the interphase dynamics causes a smoothing of the internal stress profile with increasing time and approaching the glass-transition temperature of the glassy phase, which relates to the partial cancellation of the sharp and static internal stress configurations. At $T = 350$ K the importance of the interphase dynamics becomes most apparent. The stress profile becomes almost similar in shape to the stress profile of the melt-like system computed

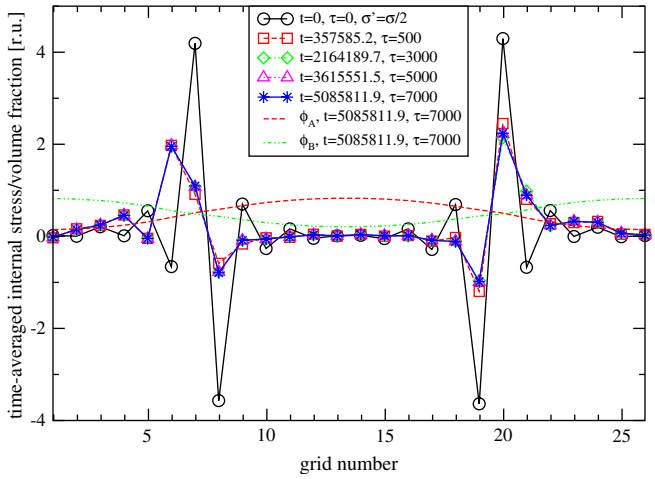

Fig. 6. Time-averaged internal stress as a function of the grid number for the TPE material composed of ABA triblock copolymers at $T = 305$ K, determined with the KMC–SCFT algorithm.

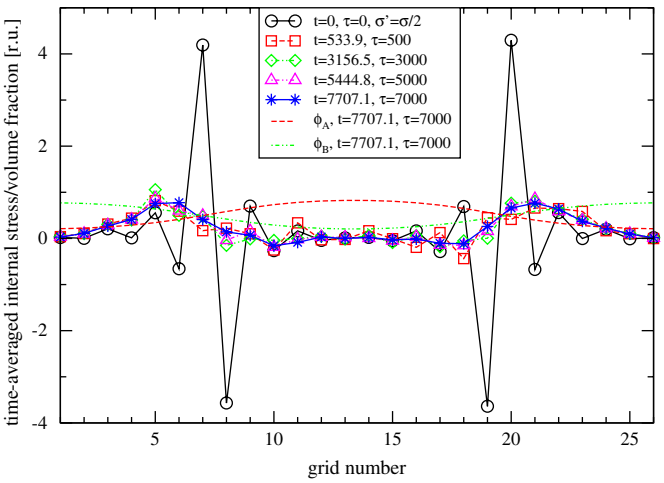

Fig. 8. Time-averaged internal stress as a function of the grid number for the TPE material composed of ABA triblock copolymers at $T = 350$ K, determined with the KMC–SCFT algorithm.

with the standard SCFT approach [25] and shown in Fig. 1. In this context, it is also worth considering that the standard SCFT approach does only take into account the transient vdW bonds acting in the glassy PS phase in a mean-field sense, whereas the KMC–SCFT approach introduces higher-order bond fluctuations. Moreover, it is important to point out that our calculation results are validated through several theoretical and experimental investigations. The implausibility of sharp interfaces at such small scales together with the presence of regions with mixed monomeric composition [50], motivated Leary and Williams to introduce the thick-interface concept, to model these systems [51]. In a later work Diamant *et al.* [8] deduced from their tensile tests on TPE samples that a linear or nonlinear mechanical perturbation provides a stress concentration, localized in the interfacial region between hard and soft nanophases. Moreover, they found that the change of various interphase characteristics with the monomeric composition has a significant effect on the local and macroscopic properties of these materials. In a subsequent work Diamant and Williams [52] explained the temperature dependence of the recovery behavior of TPE materials, subjected to a large nonlinear deformation, with the gradual change of the degree of vitrification with monomeric composition. Finally, Huy *et al.* [17] concluded from their experiments with different tapered block copolymer systems that a gradual composition profile permits a more uniform distribution of the stress at the interphases, and in this way the interphases can be tuned to act as efficient *stress absorbers*, reducing the extent of the stress transfer between the nanophases.

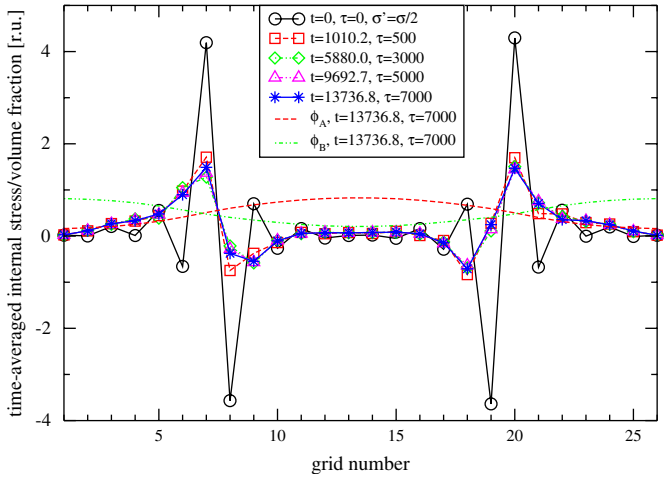

Fig. 7. Time-averaged internal stress as a function of the grid number for the TPE material composed of ABA triblock copolymers at $T = 320$ K, determined with the KMC–SCFT algorithm.

4. Conclusions

In this work we have presented a new multiscale modeling method, which combines the self-consistent field theory approach with the kinetic Monte Carlo method, and demonstrate that it is useful to simulate thermoplastic elastomers composed of triblock copolymers, which are characterized by alternating hard glassy and soft rubbery phases. In our investigation we show that on the molecular scale sharp and static glass–rubber interfaces, which experience extreme stress concentrations, are unrealistic. Moreover, we demonstrate that on this small length scale the structural properties are coupled to a chain-dynamical process, which reduces the interfacial stresses and generates a soft boundary at the interphases. In case of the styrenic block copolymer systems under investigation, we identify this process to be a thermally activated yielding process, acting in the glassy phase. In our work we demonstrate that our new methodology is capable to simulate this structural–dynamical process adequately. To show this, we apply the new methodology to a thermoplastic elastomer composed of nanophase-separated ABA triblock copolymers, and calculate its time-averaged composition and internal stress profile. We find that the structural–dynamical process generates interphases, where the degree of vitrification and the stress profile vary as a function of the monomeric composition. Moreover,

we observe that, approaching the glass-transition temperature of the glassy phase, the increasing interphase fluctuations cause an effective smoothing of the internal stress profile, due to the partial cancellation of the sharp and static internal stress configurations. At temperatures in vicinity of the glass-transition temperature, the interphase dynamics produces a stress profile similar to the one of the melt-like system. From these results, we conclude that a suitable treatment of the interphase dynamics and morphology is crucial in modeling these materials. Finally, our investigation also provides an explanation and confirms the importance of the chain-pullout mechanism, as a result of fluctuational melting, in the viscoelastic and stress relaxation behavior of these materials. Therefore, our future work will be devoted to the investigation of the influence of the chain-pullout mechanism and fluctuational melting on their mechanical behavior. Moreover, additional work will concentrate on the study of the effects of the interphase dynamics on the stress transfer between the core nanophases.

We wish to thank Glenn H. Fredrickson and Edward J. Kramer for offering helpful suggestions and encouragement. Moreover, we gratefully acknowledge the financial support of this research provided by Rhodia (France) and Mitsubishi Chemical Corporation (Japan). This work was partially supported by the MRSEC Program of the National Science Foundation under Award No. DMR 00-80034.

Appendix A. Physical picture of the glassy state within the SCFT approach

According to the Gaussian-thread model, flexible polymer chains can be represented as threads of coarse grained, spherical beads (monomers), connected by harmonic springs [25]. Despite its simplicity, the statistical mechanics required to predict the equilibrium behavior of this model is still complicated, due to the correlations associated with the interacting beads. To cope with this many-body problem, the SCFT formalism re-casts the partition function in field-theoretic formulation and re-interprets the interactions in terms of field operators. The chemical potential fields of the A and B monomers, defined as [43]

$$\begin{aligned}\widehat{w}_{\mathrm{A}}(\overrightarrow{r}) &= \chi N\widehat{\phi}_{\mathrm{B}}(\overrightarrow{r}) + \widehat{p}(\overrightarrow{r}),\\ \widehat{w}_{\mathrm{B}}(\overrightarrow{r}) &= \chi N\widehat{\phi}_{\mathrm{A}}(\overrightarrow{r}) + \widehat{p}(\overrightarrow{r}),\end{aligned} \tag{38}$$

represent the total interactions experienced by the A and B monomers at position $\overrightarrow{r}$ in space, whereas $\widehat{\phi}_A(\overrightarrow{r})$ and $\widehat{\phi}_{\mathrm{B}}(\overrightarrow{r})$ denote their respective volume fractions. In both cases the first term represents the attractive portion of the molecular interactions, while the second represents the repulsive hard-core part. The attractive (cohesive) inter-monomer interactions cause that in the block copolymer system there is a preference for similar A–A and B–B contacts over dissimilar A–B contacts. Therefore, they are responsible for the phenomenon of phase separation in the block copolymer system [7]. In contrast, the repulsive hard-core interactions are introduced by imposing the incompressibility constraint and, as a consequence, $\widehat{p}(\overrightarrow{r})$ must be considered as the Lagrange-multiplier enforcing it [43]. Having defined the interactions involved in the system, we are prevented from solving the many-body problem by the fact that the fields fluctuate, due to the correlated motion of the monomers. In SCFT one copes with the problem by invoking the mean-field approximation, which permits to replace the field operators in Eq. (38) by their respective ensemble averages. From the resulting equations, we deduce that, by imposing our constraints, the average force field acting between the monomers is frozen and kept fix under deformation in a mean-field sense, which approximately reproduces the physical picture of a glass. Finally, we point out that, up to moderate strains, the frozen average force field is sufficiently strong, to maintain the chains fixed in the glassy region, as long as the local incompressibility constrain is relaxed accordingly.

References

[1] Hawker CJ, Bosman AW, Harth E. Chem Rev 2001;101:3661–88.
[2] Matyjaszewski K, Xia J. Chem Rev 2001;101:2921–90.
[3] Kaminsky W, Tran PD, Weingarten U. Macromol Symp 2003;193:1–11; Kaminsky W, Albers I, Vathauer M. Des Monomers Polym 2002;5:155–62; Kaminsky W. Macromol Symp 2001;174:269–76.
[4] Moad G, Mayadunne RTA, Rizzardo E, Skidmore M, Thang SH. Macromol Symp 2003;192:1–12.
[5] Baeurle SA, Fredrickson GH, Gusev AA. Macromolecules 2004;37:5784–91; Baeurle SA, Martonak R, Parrinello M. J Chem Phys 2002;117:3027–39; Baeurle SA. Phys Rev Lett 2002;89:080602-1–4; Baeurle SA. J Comput Phys 2003;184:540–58; Baeurle SA. Comput Phys Commun 2003;154:111–20; Baeurle SA. Comput Phys Commun 2004;157:201–6; Baeurle SA, Efimov GV, Nogovitsin EA. J Chem Phys 2006;124:224110-1–8; Baeurle SA, Efimov GV, Nogovitsin EA. Europhys Lett 2006;75:378–84.
[6] Gusev AA. Macromolecules 2001;34:3081–93; Gusev AA. J Mech Phys Solids 1997;45:1449–54.
[7] Fredrickson GH, Ganesan V, Drolet F. Macromolecules 2002;35:16–39.
[8] Diamant J, Williams MC, Soane DS. Polym Eng Sci 1988;28:207–20.
[9] Holden G, Bishop ET, Legge R. J Polym Sci Part C 1969;26:37–57.
[10] Baeurle SA, Hotta A, Gusev AA. Polymer 2005;46:4344–54.
[11] Pukánszky B. Eur Polym J 2005;41:645–62.
[12] Sperling LH. Introduction to physical polymer science. New York: Wiley; 2001.
[13] Henderson CP, Williams MC. Polymer 1985;26:2021–5; Henderson CP, Williams MC. Polymer 1985;26:2026–38.
[14] Morèse-Séguéla B, St-Jacques M, Renaud JM, Prud'homme J. Macromolecules 1980;13:100–6.
[15] Kraus G, Rollmann KW. J Polym Sci Polym Phys Ed 1976;14:1133–48; Kumler PL, Keinath SE, Boyer RF. Polym Eng Sci 1977;17:613–21.
[16] Stöppelmann G, Gronski W, Blume A. Polymer 1990;31:1838–53.
[17] Huy TA, Hai LH, Adhikari R, Weidisch R, Michler GH, Knoll K. Polymer 2003;44:1237–45.
[18] Spontak RJ, Patel NP. Curr Opin Colloid Interface Sci 2000;5:334–41.
[19] Baeurle SA, Hotta A, Gusev AA. Polymer 2006;47:6243–53.
[20] Zhu XX, Zhu GR. Polymer 1992;33:4968–76.
[21] Lawlor A, Reagan D, McCullagh GD, De Gregorio P, Tartaglia P, Dawson KA. Phys Rev Lett 2002;89:245503-1–4; Lawlor A, De Gregorio P, Dawson KA. J Phys Condens Matter 2004;16:S4841–8.
[22] Barrat JL, Fredrickson GH, Sides SW. J Phys Chem 2005;109:6694–700.
[23] Note that the stress is made dimensionless by dividing through a factor accounting for the total number of chains $n\beta/V$, where n is the number of chains, β is the inverse temperature and V is the volume of the system [22].

[24] Doi M, Edwards SF. The theory of polymer dynamics. New York: Oxford; 1986.
[25] Sides SW, Fredrickson GH. Polymer 2003;44:5859–66.
[26] Griffith AA. Philos Trans R Soc London 1921;A221:163–98.
[27] Krausz AS, Eyring H. Deformation kinetics. New York: John Wiley & Sons; 1975; Roylance DK. Characterization of polymer deformation and fracture. In: Brame EG, editor. Applications of polymer spectroscopy. New York: Academic; 1978. p. 207–19.
[28] Swallowe GM, Lee SF. J Phys IV France 2003;110:33–8.
[29] Argon AS. Philos Mag 1973;28:839–65.
[30] Brown N. J Mater Sci 1983;18:2241–54.
[31] Hotta A, Clarke SM, Terentjev EM. Macromolecules 2002;35:271–7.
[32] Di Marzio EA, Yang AJM. J Res Natl Inst Stand Technol 1997;102: 135–57.
[33] Eyring H, Ree T. Proc Natl Acad Sci USA 1961;47:526–37; Hsu CC, Eyring H. Proc Natl Acad Sci USA 1972;69:1342–5.
[34] Cicerone MT, Blackburn FR, Ediger MD. Macromolecules 1995;28: 8224–32; Merabia S, Sotta P, Long D. Eur Phys J E 2004;15: 189–210.
[35] Matsen MW, Schick M. Phys Rev Lett 1994;72:2660–3.
[36] Michler GH, Adhikari R, Henning S. J Mater Sci 2004;39:3281–92.
[37] Bortz AB, Kalos MH, Lebowitz JL. J Comput Phys 1975;17:10–8.
[38] Gilmer GH. J Cryst Growth 1976;36:15–28; Voter AF. Phys Rev B 1986;34:6819–29; Blue JL, Beichl I, Sullivan F. Phys Rev E 1995; 51:R867–8; Block M, Kunert R, Schöll E, Boeck T, Teuber Th. New J Phys 2004;6:166-1–12; Gusev AA, Suter UW. J Chem Phys 1993;99:2228–34; Gusev AA, Arizzi S, Suter UW, Moll DJ. J Chem Phys 1993;99:2221–7.
[39] Fichthorn KA, Weinberg WH. J Chem Phys 1991;95:1090–6.
[40] Termonia Y, Meakin P, Smith P. Macromolecules 1985;18:2246–52; Termonia Y, Meakin P, Smith P. Macromolecules 1986;19:154–9; Termonia Y, Smith P. Macromolecules 1987;20:835–8; Termonia Y, Smith P. Macromolecules 1988;21:2184–9; Terzis AF, Theodorou DN, Stroeks A. Macromolecules 2002;35:508–21; Terzis AF. J Phys Conf Ser 2005;10:171–4.
[41] Allen MP, Tildesley DJ. Computer simulation of liquids. Oxford: Clarendon; 1996.
[42] Solunov CA. J Phys Condens Matter 2002;14:7297–309.
[43] Matsen MW. J Phys Condens Matter 2002;14:R21–47.
[44] Rudolf B. Macromol Chem Phys 1995;196:4057–68.
[45] Miller AA. J Polym Sci Part A2 1968;6:1161–75.
[46] van Melick HGH, Govaert LE, Meijer HEH. Polymer 2003;44: 2493–502.
[47] Zhurkov SN. Int J Fract Mech 1965;1:311–23.
[48] Beecher JF, Marker L, Bradford RD, Aggarwal SL. J Polym Sci Part C 1969;26:117–34; Smith TL. Time-dependent mechanical properties of elastomeric block polymers in large tensile deformations. In: Aggarwal SL, editor. Block polymers. New York: Plenum; 1970. p. 137–51; Robinson RA, White EFT. Mechanical properties of styrene–isoprene block copolymers. In: Aggarwal SL, editor. Block polymers. New York: Plenum; 1970. p. 123–36.
[49] Park CH, Kim JH, Ree M, Sohn BH, Jung JC, Zin WC. Polymer 2004; 45:4507–13.
[50] Shen M, Cirlin EH, Kaelble DH. J Polym Sci Polym Lett Ed 1970;8: 149–53.
[51] Leary DF, Williams MC. J Polym Sci Polym Lett Ed 1970;8:335–40; Helfand E, Wassermann ZR. Polym Eng Sci 1977;17:582–6.
[52] Diamant J, Williams MC. Polym Eng Sci 1989;29:227–34.